ChemPubSoc Europe
DOI: 10.1002/chem.201603059
CHEMISTRY A European Journal
Full Paper

Physical Chemistry

Factors Affecting the Performance of Champion Silyl-Anchor Carbazole Dye Revealed in the Femtosecond to Second Studies of Complete ADEKA-1 Sensitized Solar Cells

Jan Sobuś,[a, b] Błażej Gierczyk,[c] Gotard Burdziński,[b] Mariusz Jancelewicz,[a]
Enrico Polanski,[d, e] Anders Hagfeldt,[d] and Marcin Ziółek*[b]

Abstract: Record laboratory efficiencies of dye-sensitized solar cells have been recently reported using an alkoxysilyl-anchor dye, ADEKA-1 (over 14%). In this work we use time-resolved techniques to study the impact of key preparation factors (dye synthesis route, addition of co-adsorbent, use of cobalt-based electrolytes of different redox potential, creation of insulating Al_2O_3 layers and molecule capping passivation of the electrode) on the partial charge separation efficiencies in ADEKA-1 solar cells. We have observed that unwanted fast recombination of electrons from titania to the dye, probably associated with the orientation of the dyes on the titania surface, plays a crucial role in the performance of the cells. This recombination, taking place on the sub-ns and ns time scales, is suppressed in the optimized dye synthesis methods and upon addition of the co-adsorbent. Capping treatment significantly reduces the charge recombination between titania and electrolyte, improving the electron lifetime from tens of ms to hundreds of ms, or even to single seconds. Similar increase in electron lifetime is observed for homogenous Al_2O_3 over-layers on titania nanoparticles, however, in this case the total solar cells photocurrent is decreased due to smaller electron injection yield from the dye. Our studies should be important for a broader use of very promising silyl-anchor dyes and the further optimization and development of dye-sensitized solar cells.

Introduction

Dye-sensitized solar cells (DSSC)[1–4] represent one of the most important emerging photovoltaic technologies, which—thanks to potential inexpensiveness—have a real chance to become an alternative to the relatively expensive solar panels, dominated by inorganic silicon cells and thin film cells (mainly CdTe and CIGS), used so far. Thanks to the specific properties of DSSC such as good sunlight conversion efficiency under moderate illumination intensity, possible construction of semi-transparent systems and selection of dyes with different absorption bands, they can be used in indoor environments, in decorations or on building façades (i.e., in the so-called BIPV: building-integrated photovoltaics). However, their widespread use requires improvement of the DSSC efficiency (the highest certified one is 11.9%[5]). Another important problem to be solved is the long-term stability of DSSC devices.

Total charge separation in DSSC, the quantum yield of which determines the maximum current flowing in the solar cell, involves a few partial processes: electron injection from the dye to the semiconductor (usually titania) nanostructure, the regeneration of the oxidized dye, and charge collection from the nanostructured photoanode.[1,3,4] To ensure quantum yields of charge separation close to 100%, some excess energy is needed for partial separation processes that have to compete with the undesired pathways of charge transfer. However, the greater the excess energy (energy loss) the lower the voltage of the open circuit (V_{OC}). The value of this voltage, along with the photocurrent intensity, determines the actual efficiency of the solar cell.[1,6] For many years the dominant DSSC systems were based on ruthenium dyes and an iodide electrolyte (containing the pairs I^-/I_3^-, with multi-electron redox reaction mechanism), in which an effective process of dye regeneration

---

[a] *Dr. J. Sobuś, Dr. M. Jancelewicz*
NanoBioMedical Centre, Adam Mickiewicz University in Poznań
Umultowska 85, 61-614 Poznań (Poland)

[b] *Dr. J. Sobuś, Dr. G. Burdziński, Dr. M. Ziółek*
Quantum Electronics Laboratory, Faculty of Physics
Adam Mickiewicz University in Poznań, Umultowska 85
61-614 Poznań (Poland)
E-mail: marziol@amu.edu.pl

[c] *Dr. B. Gierczyk*
Faculty of Chemistry, Adam Mickiewicz University in Poznań
Umultowska 89b, 61-614, Poznań (Poland)

[d] *Dr. E. Polanski, Prof. A. Hagfeldt*
Laboratory of Photomolecular Science
Institute of Chemical Sciences and Engineering
École Polytechnique Fédérale de Lausanne
CH-1015, Lausanne (Switzerland)

[e] *Dr. E. Polanski*
Present address: Department of Physical Chemistry
University of Tor Vergata–Rome, Via della Ricerca Scientifica 1
00133 Rome (Italy)

Supporting information and the ORCID identification number for the author of this article can be found under http://dx.doi.org/10.1002/chem.201603059 including Figures S1–S11, Tables S1–S4 and the details of electrochemical impedance studies.

required particularly large driving force.[7–9] Recently, alternative electrolytes based on cobalt ions (with single-electron redox pair Co^{2+}/Co^{3+}) have been developed.[10–15] Their redox level is energetically lower (has more positive potential).[10–12] The use of these cobalt electrolytes in combination with organic dyes without ruthenium content, has led to higher V_{OC} values of the solar cells at similar values of photocurrent to the ones reported before. This in turn has brought laboratory efficiencies of DSSC using porphyrin dyes as high as up to 13%.[16,17] The ways to use cobalt complexes in quasi-solid electrolyte for stable DSSC have been also proposed.[18,19] Calculations suggest that the use of cobalt-based electrolytes and optimization of all parameters should theoretically bring the DSSC efficiency to almost 18% (at the total energy loss reduced to 0.4 eV in contrast to 0.75 eV for iodide electrolytes).[6] However, in the systems with cobalt electrolytes, the common problem is a fast process of undesirable recombination of electrons from the conduction band. It enforces the use of special methods for insulation of metal oxide nanoparticles from the electrolyte for the majority of applied dyes.

A novel family of dyes with silyl anchoring groups have been proposed by Japanese researchers for employment as sensitizers in DSSC.[20–24] It has been shown that the covalent bond made by the alkoxysilyl groups on the surface of the metal oxide nanoparticles (Si–O–Ti) is much stronger than the one made by the traditional carboxylic groups (C–O–Ti). Owing to this property, it was possible to apply the passivation of the metal oxide surface by few rather strong acids (called multi-capping). Their molecules fill the voids between the dye molecules and block the access of the cobalt electrolyte to the metal oxide nanoparticles. This method could not be applied for the systems with dyes comprising carboxylic groups because it resulted in the detachment of dye molecules from the nanoparticles' surface.[21] Moreover, silyl-anchor dyes, which can be used with the multi-capping technique, exhibit remarkable stability and resistance to water in DSSC devices.[21]

The best dye of this new family so far is ADEKA-1, a silyl modification of the popular carbazole sensitizer MK2.[25–28] For ADEKA-1 used alone, the best efficiency of DSSC was 12.5%,[21] and in combination with SFD-5 (another silyl-anchor dye, absorbing in more short-wavelength range of the solar spectrum) the efficiency increased to 12.8%,[23] while in co-sensitization with LEG4 (a carboxy-anchor dye with triphenylamine electron donor group) the best efficiency exceeded 14%.[24] According to our knowledge, this is a record reported laboratory efficiency of DSSC. Therefore, it is quite likely that the dyes with silyl anchoring groups in combination with cobalt electrolytes can instigate revival of the DSSC technology.

On the other hand, however, studies of DSSC employing silyl-anchor dyes have not been undertaken in other laboratories so far. One of the reasons might be difficulties with the proper dye synthesis. Moreover, no fundamental characterization of the dyes with silyl anchoring groups is available. This problem needs thorough fundamental research that would bring information about the interaction of the dyes with metal oxide nanoparticles so that the design of new DSSC would be more effective. In particular, to the best of our knowledge, no time-resolved studies have been performed for the dyes with silyl anchoring groups so far.

Therefore, in this work we employ time-resolved laser spectroscopy and electrochemical impedance spectroscopy to study the dynamics of charge transfer in complete solar cells sensitized with ADEKA-1 dye on the time scale from 200 fs to several seconds. We investigate the influence of several optimization procedures (employed for DSSC sensitized with ADEKA-1[21]) on the partial charge separation efficiencies. These additional treatments are: the incorporation of co-adsorbent, the use of cobalt-based electrolytes of different redox potentials, creation of insulating Al_2O_3 layers and passivation of the electrode by molecule capping. Moreover, we report, in more detail, the route for the most efficient (and free from polymerization problems) synthesis of ADEKA-1 and related alkoxysilyl-anchor dyes.

Results and Discussion

Effect of the synthesis route

The synthetic procedure for ADEKA-1 published previously[21] is complex in several aspects. First, the authors have reported the use of water during work-up of the reaction mixture, that is, extraction of polar byproducts with this solvent. It is well known, that alkoxysilane derivatives are highly unstable in hydrolytic conditions.[29,30] In the presence of water they undergo polycondensation (via silanol intermediate). This process is faster in the presence of ionic substances in water. As a consequence, the use of this procedure results in a mixture of ADEKA-1 and polymeric products formed during its polycondensation. Depending on the time of shaking with water and on its amount, the organic layer contains a mixture of monomeric and polymeric form of the dye or even only polymer (Figure 1). Moreover, the authors of reference [21] applied column chromatography on silica to purify the product. The second aspect of alkoxysilane chemistry is the tendency of these compounds to react with surface of silica (and other oxide materials).[31–33] The presence of silanol groups on the SiO_2 surface results in immobilization of SiOR containing molecules linked through SiOSi bond formation. This interaction strongly decreases the yield of the product. If the elution of the dye is carried out slowly, almost 100% of the monomer is covalently bonded to the silica. The fast elution allows separation of the expected fraction however it reduces its purity. Work-up of the reaction mixture according to the published procedure results in isolation of ADEKA-1 (5–10 mg) in low yields. The composition of the eluent is also important. The authors have used a mixture of chloroform/hexane (1:1 v/v). Both ADEKA-1 and MK2 dyes are basically immobile on silica in this solvent system. The use of pure diethyl ether, acetonitrile, chloroform/methanol (1:1) or chloroform/acetone (1:2) is needed to elute ADEKA-1. Therefore, in the present work we describe an upgraded synthetic procedure in the Experimental Section.

During the process of synthesis optimization several batches of ADEKA-1 were obtained, with different content of the poly-

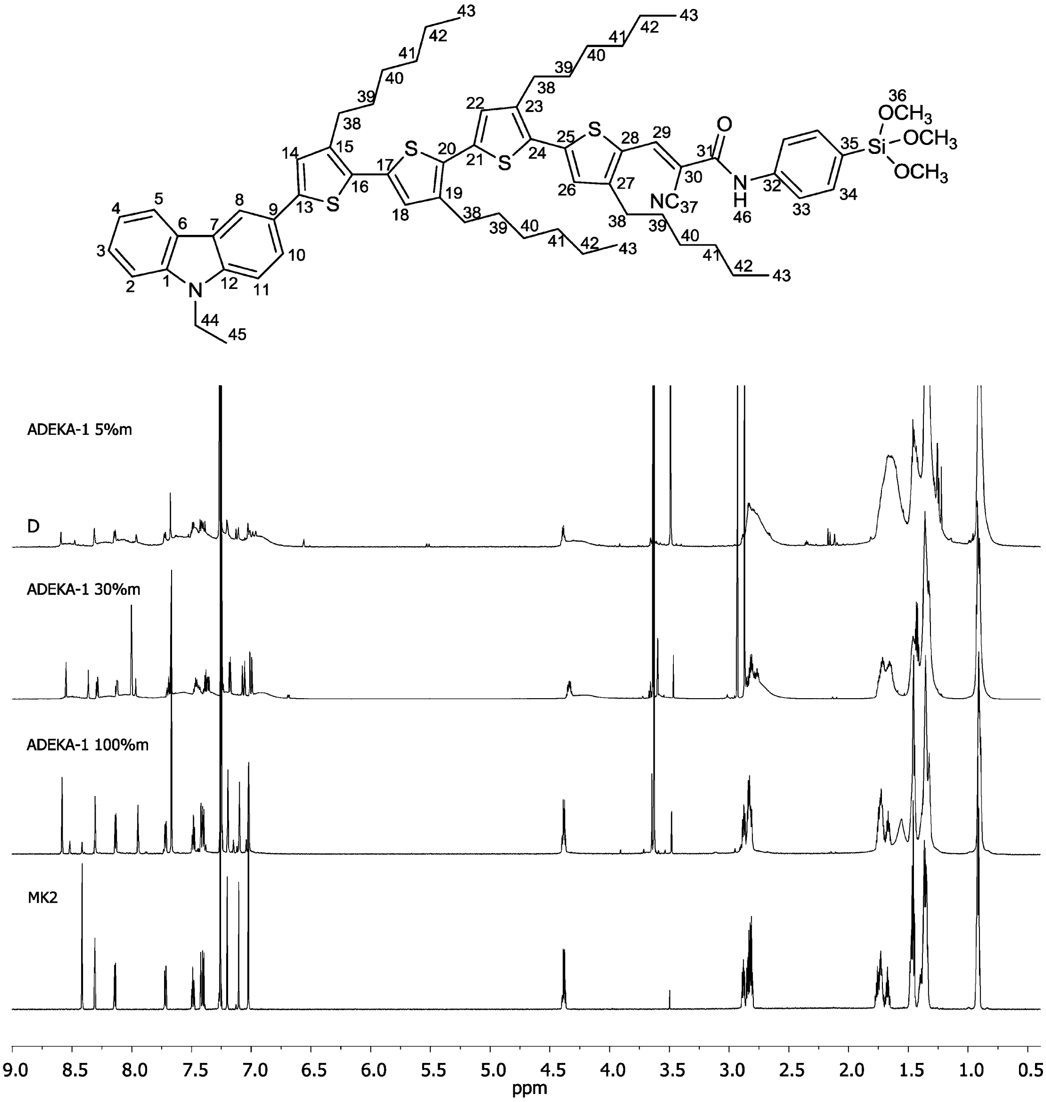

Figure 1. ADEKA-1 dye structure (top) and ^1H NMR spectra of: MK2, ADEKA-1, and partially polymerized ADEKA-1 samples (ca. 30 and 5% of monomer, respectively) in $CDCl_3$ (bottom).

merized version of the dye (ranging from purely monomer, through 50%/50% monomer/polymer mixture, to the 5%/95% monomer/polymer batch). The polymer content was verified by NMR spectroscopy in all cases. For simplicity, the samples will be named (here and in the rest of the text) according to the monomer content, for example, "60%m" means the sample consisting of 60% of monomer and 40% of polymer. The cells made with the following samples were investigated: 100%m, 100%m_old (the same sensitizing solution kept for more than 2 months), 60, 50 and 5%m. The differences in the monomer content can be also observed in the normalized stationary absorption spectra in toluene by examination of the local absorption minimum around 423 nm (Figure S3). A clear minimum is present for pure monomer synthesis (both in fresh and aged solutions), while the spectrum of polymerized dye (5%m) does not exhibit it. Moreover, it turned out that the polymerized dye has its absorption maximum moved slightly to the shorter wavelength, while the absorption tail is extended to the red. For an equal mixture of monomer and polymer, the absorption spectrum is more similar to 100%m, but the minimum at 423 nm is flattened.

General trends observed in transient absorption

Femtosecond transient absorption spectroscopy was used to measure the relative efficiency of the charge separation occurring up to 3 ns (time window of the ultrafast transient absorption setup). A simple way to test this is a comparison of the normalized kinetics probed at 750 nm. As previously reported by us for the reference MK2 dye,[34] the combined spectrum of dye radical cation and electrons in titania has a maximum close to this wavelength. On the other hand, the initial signal (just after excitation) is proportional to the population of the singlet excited state of the dye. Therefore, the magnitude of the signal left after the 3 ns (ratio of the final to initial amplitude) shows the amount of the charge carriers that were successfully separated and did not recombine with the dye molecule itself. In principle, the extinction coefficient of radical cation of monomer and polymer can be different, but assuming that the proportional difference is also maintained for the excited state of monomer and polymer (initial signal), the normalized kinetics give proper estimation of the charge separation. The selected, representative kinetics for different ADEKA-1 cells (as well as the reference kinetics for MK2 cell) are presented in Figure 2 A. As can be seen, there is a large variety of the residual amplitude for different ADEKA-1 cells, and only the best configurations match the efficiency obtained for MK2 cell.

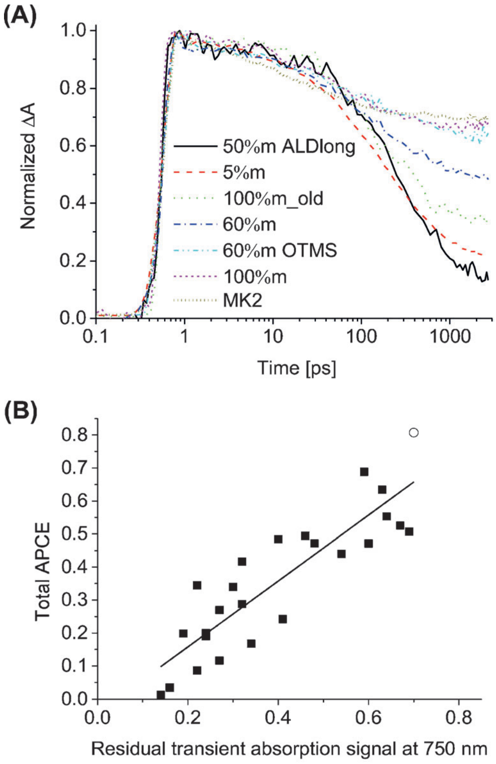

Figure 2. A) Kinetic of transient absorption traces at 750 nm of various cells sensitized with ADEKA-1 dye. Time zero was shifted to 1 ps in order to present the time axis in logarithmic scale. B) Total APCE of the various cells plotted versus the relative amplitude of residual signal at 750 nm in the transient absorption experiment measured after 3 ns after sample excitation. The detailed parameters of the cells represented by filled squares (various versions of ADEKA-1 dye, surface treatments and addition or lack of OTMS co-adsorbent) are presented in Table 1. The open circle was obtained for MK2 cell.

It should be noted that the above analysis reflects the initial charge-separation efficiency with respect to the number of absorbed photons, so it cannot be directly correlated with short-circuit current density (J_{SC}) of the cells having different number of adsorbed dyes. The global solar cell parameter that accounts for the differences in light absorption is total absorbed photon to current efficiency (APCE). This parameter was estimated by dividing the photocurrent of the full working device by the number of the photons absorbed by the dye. The number of the photons absorbed was obtained from integration of stationary absorption spectrum of the sensitized electrode (with subtracted spectrum of an unloaded electrode) and by taking into account the photon flux spectrum from AM1.5G data.

As shown in Figure 2 B and in Table 1, the amplitude of the residual signal at 750 nm corresponds well to the total APCE of the device, independently of the dye series, co-adsorbent addition and surface treatments (described later). The MK2 dye was used as a reference here due to its high efficiency on this timescale. If it can be matched by ADEKA-1 on the ultrafast timescale, the alkoxysilane bonding provides ways to prevent transport recombination on the longer timescales and improve voltage of the device (as will be shown later). Judging from Figure 2 and Table 1 one can see that the polymerized ADEKA-1 dye (5 %m) gives the lowest efficiency. The cells from the aged synthesis (100 %m_old) are marginally better. The best efficiency on the ultrafast timescale is obtained for 100 %m sample.

More detailed information was obtained from the global analysis of the transient absorption spectra. The analysis was performed in a similar way to that recently reported by us for MK2 cells.[34] The transient absorption spectra are decomposed by using four time constants plus an offset constant in the time window of an experiment. The pre-exponential factor spectra of the fitted components are shown in Figure 3 for selected samples.

The first three components were similar for all cells, so for a better comparison between different cells their average values (0.2, 3 and 40 ps) were used in the final fitting as fixed values. The fourth, sub-ns component (in the range of several hundred ps) was left as a variable one. The fastest component (0.2 ps) is comparable to the IRF of the setup and it contains significant contribution of coherent artifacts that occur during pump-probe overlap,[35] so for the sake of clarity of the presentation it is absent in the graphs. The two shortest components (0.2 and 3 ps) are attributed to the electron-injection process from the excited dyes. As can be seen in Figure 3, the pre-exponential factor spectra of the 3 ps component are usually negative in the range from 600 to 750 nm, which probably indicates the rise of the population of dye radical cation and trapped electrons in titania,[34] as well as a possible contribution of the decay of the stimulated emission from the excited state of the dye.

Longer components (40 ps and sub-ns) should probably be assigned to the fast recombination between the injected electrons and the dyes.[34,36–41] We think that the factors driving such recombination can be similar to those recently reported for DSSCs with porphyrin dyes.[42,43] As has been shown, the fast recombination rates are directly dependent on the dye molecule orientation (tilt angle) on the surface, with perpendicular molecules having longest recombination time constants.[43] Similarly to our previous assignment for MK2,[34] the 40 ps component represents the recombination between the electrons injected to the trap states (yet to be successfully separated) and the dye. For all ADEKA-1 cells the amplitude of the 40 ps component mirrors the 3 ps one, and their relative ratio is independent from the cell efficiency. On the contrary, the

Table 1. Photovoltaic parameters of representative cells used for femtosecond transient absorption studies.[a]

Cell	V_{OC} [V]	FF	J_{SC} [mAcm^{-2}]	Eff. [%]	Nph [10^{20} s^{-1} m^{-2}]	A_{max}	Total APCE	S_{res}
100 % m_old + OTMS	0.70	0.46	3.60	1.16	5.4	0.71	0.42	0.32
100 % m_old + OTMS + ALD"short"	0.62	0.37	2.16	0.50	5.0	0.58	0.27	0.27
100 % m_old + OTMS + multi-capping	0.67	0.61	2.95	1.19	3.8	0.48	0.48	0.40
100 % m_old + OTMS + ALD"long"	0.85	0.59	2.28	1.14	7.2	1.22	0.20	0.19
5 % m	0.61	0.52	1.17	0.37	8.5	1.56	0.09	0.22
5 % m + OTMS	0.61	0.66	1.27	0.51	6.8	1.04	0.12	0.27
50 % m	0.74	0.54	7.35	2.92	9.3	1.70	0.49	0.46
50 % m + OTMS	0.72	0.50	6.57	2.39	8.1	1.43	0.51	0.69
50 % m + OTMS + multi-capping	0.70	0.59	4.22	1.75	6.0	0.85	0.44	0.54
50 % m + OTMS + ALD"short"	0.73	0.48	8.59	3.02	7.8	1.40	0.69	0.59
50 % m + OTMS + ALD"long"	0.92	0.80	0.16	0.12	7.6	1.54	0.01	0.14
60 % m	0.72	0.50	6.87	2.44	9.1	1.56	0.47	0.48
60 % m + OTMS	0.70	0.55	7.43	2.87	8.4	1.50	0.55	0.64
60 % m + OTMS + multi-capping	0.69	0.66	4.83	2.20	6.4	0.90	0.47	0.60
100 % m	0.71	0.54	6.98	2.70	8.3	1.32	0.53	0.67
MK2	0.72	0.45	11.24	3.64	8.7	1.51	0.81	0.70

[a] Photocurrent density (J_{SC}), open circuit voltage (V_{OC}), fill factor (FF), efficiency (Eff.), corrected photoconversion efficiency (total APCE), absorbance of the cells close to the maximum (at 500 nm, A_{max}), number of absorbed photons (Nph), and the amplitude of the normalized residual signal of kinetic at 750 nm (S_{res}, ratio of the amplitude after 3 ns to the initial one).

"sub-ns" and constant offset components vary a lot for the cells of different performance. Therefore, we think that the sub-ns component represents the recombination of the injected electrons with the dye between the free electrons in titania and the donor part of the dye molecule. Since it competes with the constant offset signal of the successfully separated oxidized dyes and charge carriers, the low amplitude of sub-ns component and its red shift is mostly beneficial for the successful charge separation.

It is clearly visible from Figure 3 that the polymerized version (5 % m) has the highest amplitude of the sub-ns signal compared to the blue residual one. The aged dyes also exhibit higher sub-ns signal than the constant offset one. This means that in both cases the unwanted recombination has the highest contribution. At the moment, we do not have a clear explanation why the aged 100 % m solution gives a much worse performance then the fresh one, since both stationary absorption (Figure S3) and NMR analysis do not reveal any differences in the signals of ADEKA-1. One explanation might be that the dye can suffer from isomerization over time which facilitates recombination due to closer orientation towards the nanoparticle surface. Another possibility might be that older solution enhanced formation of dye aggregates on titania surface. Moving to the 50 % m and 60 % m synthesis, the recombination signal is suppressed successfully. Increasing the monomer content by 10 % makes the recombination signal even lower and extends it characteristic time by 100 ps. The optimized synthesis process (100 % m) results in the lowest amplitude of the sub-ns component and the position where its spectrum changes the sign from negative to positive (intersection with $\Delta A = 0$ line) shifts as far as 670 nm. The red shift of the negative amplitude in the sub-ns component in efficient cells might be due to the Stark shift effect.[44–46] As more electrons are fully separated in better cells, they create larger electric field on the nanoparticle surface. It leads to enhanced negative signal due to the Stark shift of dye absorption band. Another possibility is that in better cells the orientation of molecules is more perpendicular to the surface, which makes the direction of the ADEKA-1 dipole moment better aligned with electric field direction, and in turn enhances the Stark shift effect as well.[44–46]

Selected fully assembled cells were also probed with transient absorption measurements in ns–μs timescale. Resulting kinetics were analyzed by using global fitting multi-exponential function. The resultant time constants with the wavelength-dependent amplitudes (associated with each time constant) are shown in Figure 4 A–C. Besides the three components shown in the figures, an additional 20 ns component (IRF of the setup) was also used in the fit to account for the scattered laser excitation light. Two shorter components (around 200 ns and 3.5–4 μs) represent the decay of the oxidized dye molecules (radical cation) due to electron-dye recombination and dye regeneration (by electrolyte). Their spectra can be divided into two parts. The positive part corresponds to the absorption of oxidized dye. The negative one shows disappearing depletion of the ground state of dye molecules (bleach signal) and a possible contribution from the Stark shift effect. The longest time, having positive amplitude over all wavelengths, represents absorption of electrons left in titania.[47,48]

The results for reference MK2 cells (Figure 4 A) are similar to the ones in our previous paper,[34] but in that report we resolved one averaged short component (about 1 μs), assigned to dye regeneration dynamics. Here we find that this component should rather be divided into two contributions (200 ns and 4 μs) of slightly different pre-exponential factor spectra. Most probably, the faster one contains a significant part of electron-dye recombination, which might be a continuation of the sub-ns recombination observed in ultrafast transient experiments (lowering the performance of the solar cell). Indeed, for the ADEKA-1 cell with the poor efficiency (Figure 4 B, old solution) the contribution of the 200 ns component is higher than that in the better cell (Figure 4 C). At the same time, the amplitude of the final component (due to the electrons left in

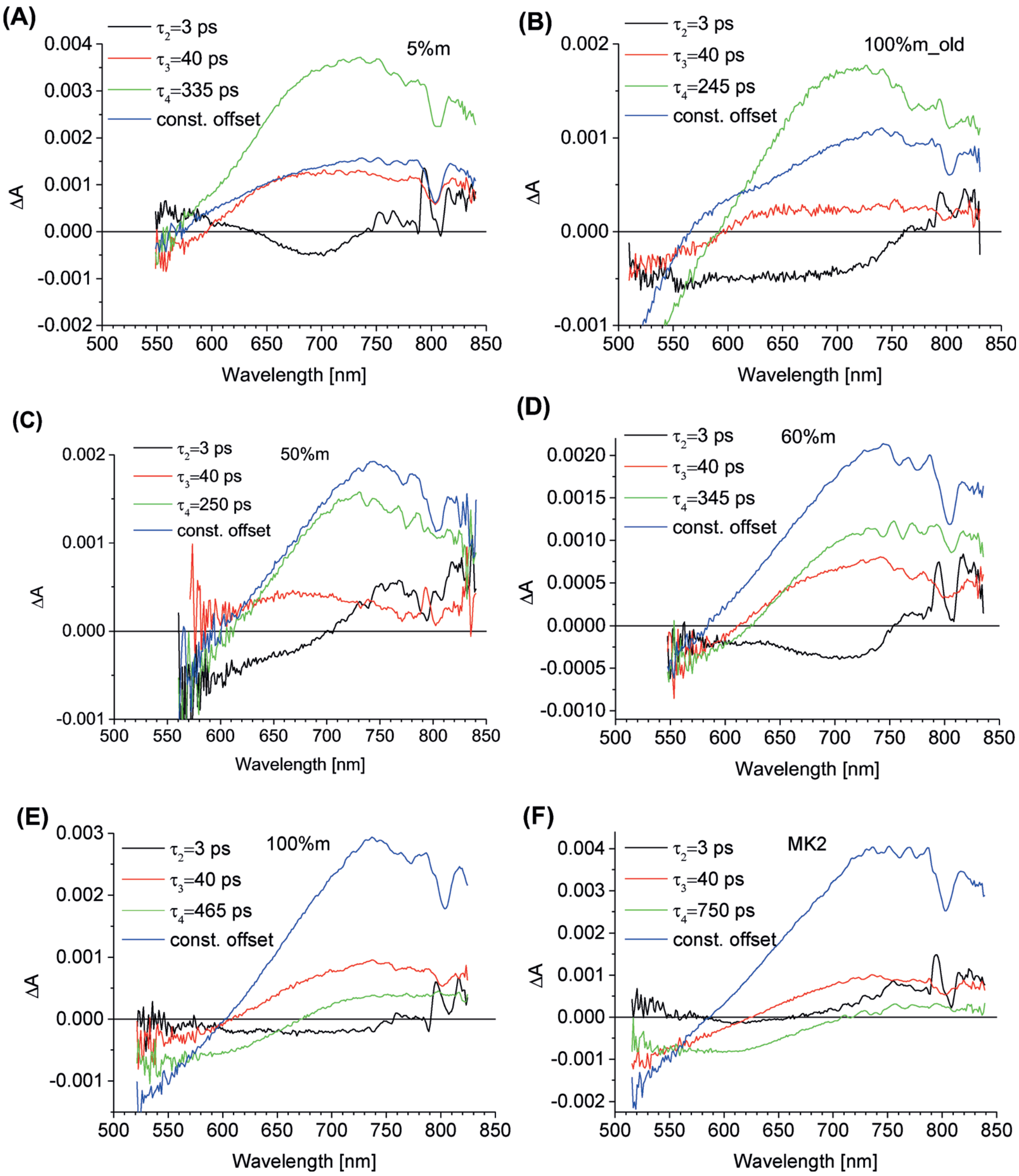

Figure 3. Wavelength dependent amplitudes of the indicated time constants obtained from global analysis of transient absorption spectra of full cells sensitized with various versions of ADEKA-1: A) 5 % m, B) 100 % m_old, C) 50 % m, D) 60 % m, E) 100 % m, F) data obtained for the reference MK2.

titania) is lower in the former than in the latter cell. Moreover, the effect of the pump pulse intensity investigated for the normalized kinetics at 750 nm (Figure 4 D) confirms this assignment. As a result of higher pump intensity (thus higher population of injected electrons and oxidized dyes per nanoparticle) the contribution of the fast component increases (as expected for the recombination process), while the dynamics of the middle, microsecond component is unchanged. Therefore, the latter can be assigned exclusively to the dye-regeneration process.

To summarize this section, we have observed that fast recombination plays a crucial role in the performance of the solar cells with ADEKA-1 dye. The unwanted dye recombination, probably associated with the orientation of the dyes on the titania surface, takes place on the sub-ns and ns time scales. Its amount is correlated with the photocurrent of the cells corrected for the number of adsorbed dyes (total APCE). The cells with higher monomer content give smaller recombination and better performance. Enhanced recombination in ADEKA-1 compared to the reference MK2 dye can probably be explained by higher electronic coupling between dye and titania (due to different anchoring groups) and/or additional molecule rotation possibilities present in the extended anchoring group of ADEKA-1. In the next sections, the influence of other factors on the recombination dynamics will be presented. They include the effect of different levels of the redox couple potential, the addition of co-adsorbent, capping treatment and the effect of alumina protection layer. Besides the fs–μs laser spectroscopies, electrochemical impedance spectroscopy will also be employed to test the charge-separation dynamics occurring on longer time scales.

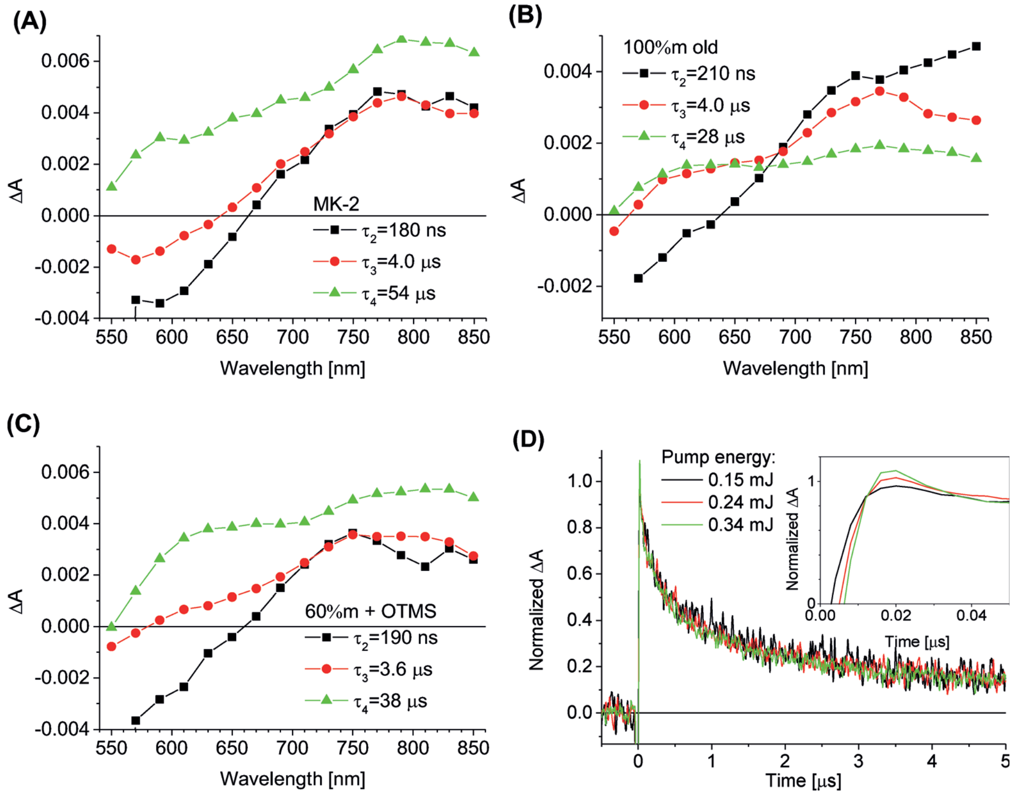

Figure 4. A–C) Wavelength-dependent amplitudes with the indicated time constants obtained from the global fit to the flash photolysis results of the MK2 and ADEKA-1 cells. D) Kinetics at 750 nm obtained in flash photolysis experiments for ADEKA-1 cell and the indicated pump-pulse energies. Inset: the initial signal over a shorter time scale.

Effects of cobalt complex, co-adsorbent and surface treatment

For selected MK2 and ADEKA-1 cells we checked the effect of changing the electrolyte redox pair from cobalt-phenenatroline (Co-phen) to cobalt-bypyridine (Co-bpy). The reason behind it was to check the effect of shifting the position of electrolyte redox potential (from 0.62 V vs. NHE for Co-phen to 0.56 V vs. NHE for Co-bpy) on the observed charge separation dynamics. The macroscopic parameters were affected in the way analogous to that frequently reported:[1,3,4] for more positive redox potential the V_{OC} of the cell increases, but at some point the J_{SC} start to decrease due to not sufficiently fast dye regeneration. Photovoltaic parameters of an example set of MK2 and ADEKA-1 cells are presented in Table S1. As can be seen, use of Co-phen instead of Co-bpy yields about 20 mV higher voltage at the expense of about 1 $mA\,cm^{-2}$ lower photocurrent. Similar effects were observed for ADEKA-1 cells (in a few configurations for which the redox couple effect was measured): lower V_{OC} by about 20–30 mV and higher J_{SC} by about 10–20%, when Co-phen is replaced with Co-bpy.

Within experimental error, no differences were observed between the ultrafast transient absorption results of the cells filled with the two cobalt electrolytes, both for MK2 and ADEKA-1. This could be expected as the position of the electrolyte redox potential should not influence either electron injection or electron-dye recombination dynamics. On the contrary, nanosecond flash photolysis measurements revealed the difference in the dye regeneration time constant (Figure S6). For MK2 cells, the middle component in the global analysis (see previous section and Figure 4) was equal to 4 µs for Co-phen and 3 µs for Co-bpy. Similar shortening of the regeneration kinetics was observed for ADEKA-1 cells—the averaged time constants decreased from 3.5 µs for Co-phen to 2.5 µs for Co-bpy. For both dyes this effect can be attributed to the larger driving force for the dye-regeneration process when bipyridine redox complex is used with respect to the phenenatroline one. On the other hand, the differences in the fitted time constants between both Co complexes are not large. However, bearing in mind the discovered fast recombination (with the time scales shorter than regeneration dynamics), even small improvements in the shortening of regeneration time constant might be responsible for the evident increase in J_{SC} of the cells.

A common method used to improve the efficiency of the device is the addition of a co-adsorbent to the dye solution. It decreases dye agglomeration and increases average distance between dye molecules, which in turn reduces the energy transfer between them.[49,50] It can also help in arranging the dye molecules perpendicularly to the oxide surface, which reduces the recombination of electrons from titania to the oxidized dye, in a way that was previously reported for porphyrin dyes.[42,43] The absorbance was compared for the photoanodes sensitized with the dye solutions with and without addition of the OTMS (Figure S4). The number of absorbed photons is reduced upon addition of OTMS by 10–20 % (Table 1).

Figure 5 A shows the global analysis spectrum of the 50 % m cell after addition of OTMS as a co-adsorbent (analogous plot for and 60 % m cell is shown in Figure S7 A). Indeed, the sub-ns recombination component is heavily reduced and the residual one (constant offset) is improved in both cases (to be compared with Figure 3 within of the same synthesis series, but without OTMS). Moreover, the sub-ns spectrum is moved a little to the red and the characteristic time is vastly increased. This most likely indicates that adsorption of OTMS molecules on titania surface takes up empty spaces between dye molecules and prevents their "tiling" on the surface, consequently reducing recombination. The overall positive impact of the addition of OTMS on the sub-ns processes is also reflected by the higher residual signal of the kinetics at 750 nm for the samples containing OTMS, compared to their counterparts without it (e.g., Figure 2 A for 60 % m).

With all the above results in hand, the differences in initial charge separation between MK2 and ADEKA-1 molecules can be compared based on the analysis of their structure and the results of previously reported molecular modeling. LUMO orbital is localized close to cyano and amide groups. The optical transition of ADEKA-1 in the visible region ($S_0 \rightarrow S_1$) consists mainly of the transition from HOMO to LUMO (77 %) and HOMO−1 to LUMO orbitals (11 %).[24] HOMO orbital is localized on the three thiophene groups closest to the carbazole group, while the HOMO−1 orbital is localized mainly on the carbazole group.[24] Therefore, these groups are the electron-donor parts of ADEKA-1, and their distance from titania surface is probably crucial for the occurrence of sub-ns recombination. Unlike MK2, ADEKA-1 can suffer from the rotation around C31−N amide bond (Figure 1 A) of a partial double bond character. It can result in the twisted structure with carbazole and next thiophene groups laying closer to the injected electrons on TiO_2 surface and enhance back electron transfer. The above rotation takes place easier in the absence of co-adsorbent molecules and for more polymerized content of ADEKA-1, in agreement with the findings of transient absorption experiments.

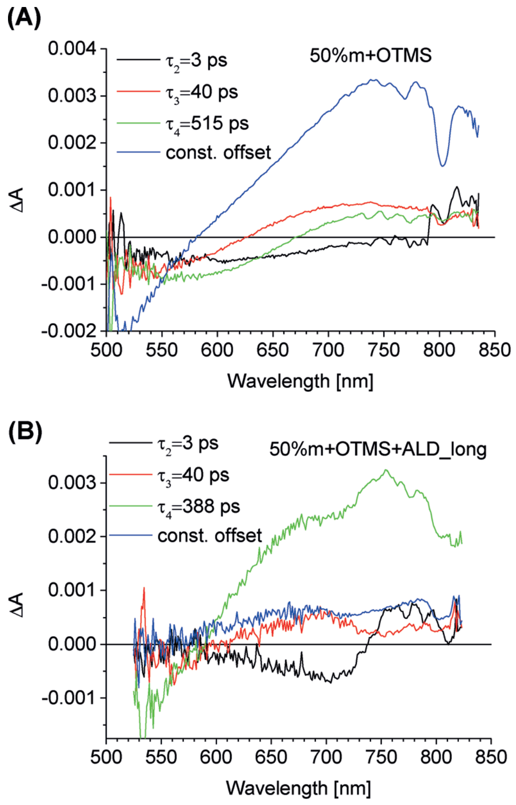

Figure 5. Wavelength dependent amplitudes of the indicated time constants obtained from global analysis of transient absorption spectra of full cells sensitized with ADEKA-1 dye and addition of OTMS: A) 50 % m, B) 50 % m with additional "long" ALD treatment. Panel A can be compared to the corresponding samples without OTMS presented in Figure 3 C.

Femtosecond transient absorption spectroscopy was also used to determine the impact of the capping process (single- and multi-capping was analyzed) and alumina shell created by the ALD process. Multi-capping sometimes increases or decreases the residual signal at 750 nm compared to cells with just OTMS present (Table 1). The positive action for the early time behavior is observed in "bad" performing cells, while the opposite is found for "good" cells (sensitized with fresh solutions of high monomer-content and with OMTS). As described earlier, OTMS probably acts to straighten the dye molecules perpendicularly to the surface and capping may act in a similar way. In the cells with a suboptimal dye orientation, it helps to set dye molecules more perpendicular to the surface, thus reducing recombination and improving the final signal. In the cells with optimal dye orientation, capping treatment may cause slight unbalance in the system, marginally lowering the final signal.

As for the ALD utilized in the photoanode preparation, we observed crucial importance of the deposition settings. The impact of these parameters has recently been investigated for planar structures.[51] In order to investigate the effect of partial ALD coating, cells were prepared with longer and shorter deposition and purging times. The details of the comparison are presented in Supporting Information. Only the "long" method was able to form uniform monolayer of alumina. For the cells with "long" ALD treatment a very profound recombination (sub-ns component) signal and low residual (constant offset component) signal was observed in transient absorption experiments (Figure 5 B). This can be explained by the blocking of electron injection from dye to titania material by 1 nm Al_2O_3 layer, probably causing significant recombination from the electrons trapped in surface states of Al_2O_3 localized close to the oxidized dyes. These observations are further supported by a residual signal in the kinetics from Figure 2 A (a huge drop in final kinetic amplitude for the "long" ALD treatment). On the contrary, "short" ALD method, similarly to the capping treatment, has no significant effect on the ultrafast processes (Figure S7 B).

Electrochemical impedance spectroscopy was used to study the effects of co-adsorbent and various kinds of surface treatment on the longer-time-scale charge separation. A detailed presentation of the results is provided in the Supporting Information. Briefly, slightly increased transport resistance and small conduction band shift occur after addition of OTMS (Figure S9 B). As a result, the decrease of the photocurrent for the cells with OTMS (Table 1 and Table S2) can be explained by the combined action of a smaller number of absorbed photons and increased transport resistance. However, in the full optimized cell (when light absorption is improved due to increased TiO_2 thickness and/or additional scattering layers) the overall impact of OTMS should be positive due to decreased sub-ns recombination.

Both molecular capping and creation of insulating Al_2O_3 layers were found to increase the lifetime of electrons significantly increasing the charge-collection efficiency beyond 90%. Moreover, the capping treatment causes slight shift in conduction band in the opposite direction compared to OTMS. The Al_2O_3 layer on the other hand causes voltage and fill-factor improvements, but at the expense of photocurrent drop. Capping treatment significantly reduces the charge recombination between titania and electrolyte: the electron lifetime is about 10 times longer for the cells with a single-capping (with respect to the cells with no capping), and further 3–5 times longer for the cells with a multi-capping (Figure S11 C). Similar increase in electron lifetime is observed for homogenous Al_2O_3 over-layers on titania nanoparticles ("long" ALD), about 2 times per 0.2 nm thickness of the layer (Figure S10 C). However, the positive effect of insulating layer on the titania-electrolyte recombination is offset by much lower initial charge-separation efficiency, which results in significantly worse global performance of the cells with homogenous Al_2O_3 over-layers.

Conclusions

The dynamics of charge transfer in complete solar cells sensitized with very efficient silyl-anchor ADEKA-1 dye (with different preparation parameters) were studied on the time scale from 200 fs to several seconds. We have also devised a new, optimized synthesis process for ADEKA-1 dye providing pure monomer compound with high yield.

The most important conclusions arise from the transient absorption spectroscopy results in the fs–ps regime. In this work we have shown that there is a time component in the global analysis of these spectra that can be directly connected with the photon to current conversion efficiency. It is associated with the undesired ultrafast recombination between dye molecule and oxide surface with characteristic time of hundreds of picoseconds (sub-ns). With its increase in amplitude, the number of successfully injected electrons falls down, directly lowering the performance of the whole device. We have proved that in the case of the ADEKA-1 dye an increase in the degree of polymerization of the dye leads to increase of this unwanted recombination. Therefore, pure monomers in the dye solution are desirable for the best performing devices. Addition of the co-adsorbent (OTMS) was found to decrease the unwanted sub-ns recombination component as well, probably by reorientation of the tilt of dye molecules on the surface of the oxide. Creation of the uniform alumina shell led to decreased efficiency of initial charge separation, with the amplitude of sub-ns recombination component significantly increased.

Secondly, flash photolysis measurements have shown that there is also a connection between performance of the device and relative amplitude of the observed time components—the shortest one (assigned to sub-μs electron recombination) and the longest one (assigned to electron population left in TiO_2). The dominance of the latter indicates a well performing device. It has also been confirmed that a Co-phenenatroline redox shuttle yields higher voltages than a Co-bipyridine one, but at the expense of a photocurrent drop, which is the result of slightly slower (3.5 vs. 2.5 μs) dye regeneration.

Next, electrochemical impedance spectroscopy has provided information about the impact of the surface treatments on the electron transport and recombination between titania and electrolyte. Both molecular capping and creation of insulating Al_2O_3 layers were found to increase the lifetime of electrons. Moreover, the capping treatment causes slight (up to 55 mV) shift in conduction band. Finally, we have underlined the importance of the parameters used during the atomic layer deposition of alumina shell, which may lead to disparate results affecting the properties of the device in an unexpected way.

We believe that these results will enable better understanding of alkoxysilyl dyes and lead to development of better DSSCs in general.

Experimental Section

Dye synthesis

Chemical compounds and apparatus used

All solvents were dried with molecular sieves (3 Å, 20% m/v). Reactions were conducted in flame-dried glassware under argon atmosphere. Dimethylformamide (DMF) was allowed to stand over CaH_2 for 24 h and distilled under reduced pressure immediately prior to use.

^1H and ^{13}C NMR spectra were recorded at 298 K on an Agilent DD2 800 spectrometer, operating at frequencies 799.926 and 201.162 MHz, respectively, equipped with $^1H[^{13}C/^{15}N]$ triple resonance probe (90° pulse width: ^1H: 13.6 μs; ^{13}C: 6.9 μs). The sample concentrations were 0.01 M. The 1D spectra were recorded by using standard one-pulse sequence (s2pul), 2D experiments were made using standard sequences with gradient pulses (gCOSY, gHMQCAD, gHMBCAD). The ^{13}C NMR spectra were recorded with broadband ^1H decoupling. Elementary analyses were performed on a Vario EL III analyzer. FT-IR spectra were recorded on a Bruker IFS 66 s spectrometer in KBr disc (1 mg in 200 mg KBr).

Synthesis process

To a stirred solution of 100 mg of MK2 dye (0.105 mmol) in 2 mL of chloroform, a solution of 14.6 mg oxalyl chloride (0.115 mmol) in the same solvent (200 μL) was added, followed by addition of 100 μL of DMF. After 1 h the mixture was cooled to 0°C and the solutions of 4-(trimethoxysilyl)aniline (22.3 mg, 0.105 mmol) and ethyldiisopropylamine (27.1 mg, 0.210 mmol) in chloroform (200 μL) were added. The mixture was then mixed for 2 h at room temperature. After the solvent was evaporated, the solid residue was dissolved in 1 mL of chloroform and 50 mL of methanol was added. The solid, blackish product was filtered off, washed with methanol and dried in vacuum. Yield is 110 mg (91%). ^{1}H NMR ($CDCl_3$): $\delta=8.59$ (1H, s; H-29); 8.31 (1H, d, $J=1.7$ Hz; H-8); 8.14 (1H, d, $J=7.4$ Hz; H-5); 7.96 (1H, s; H-46); 7.72 (1H, dd, $J=8.4$, 1.7 Hz; H-10); 7.68 (4H, s; H-33 & 34); 7.49 (1H, dd, $J=8.1$, 7.5 Hz; H-3); 7.42 (1H, d, $J=8.1$ Hz; H-2); 7.41 (1H, d, $J=8.4$ Hz; H-11); 7.26 (1H, t, $J=7.4$ Hz; H-4); 7.20 (1H, s; H-14); 7.11 (1H, s; H-26); 7.03 (1H, s; H-18 or H-22); 7.02 (1H, s; H-18 or H-22); 4.39 (2H, q, $J=7.3$ Hz; H-44); 3.64 (9H, s; H-36); 2.86 (8H, m; H-38); 1.71 (8H, m; H-39); 1.46 (16H, m; H-40 & 41); 1.46 (3H, t, $J=7.3$ Hz; H-45); 1.34 (8H, m; H-42); 0.91 ppm (12H, m; H-43). ^{13}C NMR ($CDCl_3$): $\delta=$ 155.54 (C-31); 151.4 (C-30); 144.8 (C-25); 143.6 (C-13); 142.7 (C-29); 140.9 & 143.3 (C-17 & 21); 140.8 (C-16); 140.4 (C-1); 139.6 (C-12); 135.9 (C-34); 135.4 & 136.8 (C-20 & 24); 129.8 (C-27); 129.2 (C-28); 128.9 & 129.1 (C-19 & 23); 129.0 & 128.3 (C-18 & 22); 128.5 (C-15); 127.4 (C-26); 126.0 (C-3); 125.7 (C-32 & 35); 125.4 (C-9); 125.1 (C-14); 123.9 (C-10); 123.4 (C-7); 122.8 (C-6); 120.6 (C-5); 119.5 (C-33); 119.1 (C-4); 117.9 (C-37); 117.6 (C-29); 108.8 & 108.7 (H-2 & H-11); 50.9 (C-36); 37.7 (C-44); 28.0–32.0 (C-38, 39, 40 & 41); 22.6 (C-42); 14.1 (C-43); 13.6 ppm (C-45). IR (KBr): $\tilde{\nu}=3440$, 3415, 2928, 2852, 2195, 1683, 1569, 1513, 1491, 1418, 1315, 1196, 1085, 825, 801, 724 cm^{-1}. Elemental analysis: calculated: C 69.93, H 7.27, N 3.65, S 11.15; found: C 70.02, H 7.35, N 3.59, S 11.05. ADEKA-1 structure and atom numbering are shown in Figure 1. ^{1}H-^{13}C HSQC and IR spectra are shown in Figures S1 and S2 (in the Supporting Information).

Cell preparation

Preparation of the photoanode

Glass plates of the size 16×14 mm^2 were cut from the FTO glass sheet (solar 4 mm thickness, 10 $\Omega\,sq^{-1}$, Nippon Sheet Glass, Japan). They were cleaned by using a solution of 2 g Degonex detergent in 1 L of water in an ultrasonic bath for 45 min. Afterwards, they were further purified by treatment in a UV-O_3 system (Model No. 256–220, Jelight Company, Inc.) for 15 min. Next they were submerged in a 40 mM aqueous solution of $TiCl_4$ for 40 min in 70 °C, and then rinsed in water and ethanol. Subsequently, an approximately 8 μm thick layer of mesoporous titania was deposited by screen printing twice (54T, Estal Mono, Schweiz, Seidengazefabrik, AG, Thal) using the commercially available screen-printing pastes (30NR-D or 18NR-T, Dyesol) with 8 min paste settling on 125 °C hotplate after the first print. No scattering layer was used, since it would prohibit transient absorption studies and complicate the interpretation of impedance analysis. After printing and verifying thickness by the needle profilometry, the photoanodes were again subjected to $TiCl_4$ treatment described before with the concentration lowered to 20 mM. Finally, the electrodes with the TiO_2 pastes were gradually heated under an airflow at 125 °C for 5 min, 325 °C for 5 min, at 375 °C for 5 min, at 450 °C for 15 min, and at 500 °C for 15 min.

Counter electrode preparation

Counter electrodes were prepared by cutting 18×14 mm^2 plates from the FTO-covered glass sheet (LOF Industries, TEC 15 $\Omega\,sq^{-1}$, 2.2 mm thickness) and had 1 mm conical holes sand-blasted in them. Afterwards they were cleaned in water and acetone and dried. Heating to 400 °C for 30 min in order to remove any organic contamination left was followed by drop-wise deposition of 80 μL of graphene nanoplatelets solution (1 mg per 2 mL of acetone). Upon drying in low humidity conditions it resulted in a uniform carbon layer on the glass surface.

Dye deposition

Prior to dye deposition, the photoanodes were dried in 400 °C for 30 min to remove any residual water or other contaminants. Unless otherwise indicated the dye solution had a concentration of 0.2 mM, the solvent used was toluene (dyes without co-adsorbent) or 9:1 mixture of toluene and acetonitrile (dyes with co-adsorbent). The dyes used were MK2 (Sigma) and ADEKA-1 (synthesis route described above). The co-adsorbent used was isooctyltrimethoxysilane (OTMS, Sigma–Aldrich) with concentration of 0.1 or 0.2 mM. Working electrodes were placed in the dye solution and stored at 5 °C for 16–20 h to enable efficient adsorption of the dye.

Cell assembly

Both electrodes were connected together by using a polymer seal (25 μm Surlyn, Meltronix, Solaronix SA) with conducting surfaces facing inwards. They were then filled with electrolyte through the holes in the counter electrode and sealed with the cover glass on top. The electrolyte consisted of 0.25 M Co^{2+} bis(trifluoromethane)-sulfonimide (TFSI), 0.035 M of Co^{3+}TFSI, 0.1 M of LiTFSI and 0.5 M *tert*-butylpyridine (TBP). The cobalt redox couple used was cobalt-phenantroline (Co-phen) in most cases (if not stated otherwise). For comparison studies, some cells were prepared with cobalt-bipyridine complexes (Co-bpy).

ALD and capping treatment

In some of the cells additional preparation steps were involved in order to make core-shell structures or incorporate the capping treatment. Alumina shell was deposited on the photoanodes before submerging them in the dye by using the atomic layer deposition (ALD) technique. It was performed using R-200 reactor (Picosun) with deionized water and trimethylaluminium as oxygen and aluminium sources, respectively. The duration of the deposition (0.1 or 2 s) and purge (3 or 8 s) steps of the cycle were highly important. The capping treatment was performed by sequentially dipping the photoanodes in the appropriate solutions and rinsing them with toluene, just after taking them out from the dye solution and right before cell assembly. All capping solutions had 1 mM concentration in 1:1 toluene/acetonitrile solvent. For a single-capping treatment the electrode was submerged in heptanoic acid solutions for 30 min. For multi-capping treatment it was dipped in *n*-octadecyl succinic acid for 10 min, *n*-hexadecyl malonic acid for 10 min, tetradecylphosphonic acid for 5 min, octylphosphonic acid for 5 min, heptanoic acid for 10 min and finally ethylphosphonic acid for 5 min.

Cell characterization

Current–voltage characterization of the solar cell was performed with a potentiostat (model M101 with a frequency response analyzer FRA32M module, Autolab) coupled to a photoelectric spectrometer equipped with the option of solar simulator (Photon Institute, Poland). The sunlight conditions were simulated with a Xe lamp with AM 1.5 G spectral filter and intensity adjusted to 100 $mW\,cm^{-2}$ using a calibrated silicon cell (RR-74, Rera Systems). It was used to obtain characteristics of the cells subjected to transient absorption measurements. Part of the current voltage characterization was done on a solar simulator equipped with a 450 W xenon lamp (Model No. 81172, Oriel) calibrated by using a reference Si photodiode equipped with an IR-cutoff filter (KG-3, Schott) as well (cells to be later analyzed by EIS). Electrochemical impedance spectroscopy (EIS) measurements were performed using SP-300 potentiostat (BioLogic) over the range from 0.1 Hz to 7 MHz spread in 80 measuring points distributed evenly on the logarithmic frequency scale. The obtained curves were analyzed by using the ZView software using the transmission line element.[52] More information about the voltage range and equivalent circuits is presented in the Supporting Information.

All transient absorption studies were performed for fully assembled, working solar cells (the same as those characterized in current–voltage measurements). The setup for ultrafast broadband transient absorption has been described before (Helios spectrometer, Ultrafast Systems, and Spectra Physics laser system).[53] The pump pulses were set at 500 nm and the IRF (pump-probe cross correlation function) was about 250 fs (FWHM). The pump pulse energy of 60 nJ corresponds to energy density of about 30 μJ cm^{-2}. The transient absorption measurements were performed in the spectral range of 450–850 nm and in the time range of up to 3 ns. The nanosecond flash photolysis setup was based on Q-switched Nd:YAG laser and a 150 W xenon arc lamp as the excitation and the probing light sources, respectively.[46] The pump pulse wavelength was set at 532 nm and the energy was set at 0.15 mJ (energy density of about 300 μJ cm^{-2}).

The global analysis of the transient absorption data was performed by using Surface Explorer software (Ultrafast Systems) and Asufit program[54] for ultrafast transient absorption and nanosecond flash photolysis, respectively. Both programs fit a multi-exponential function (convoluted with IRF) to either the kinetic vectors of a selected number of singular values (Surface Explorer) or to the kinetic traces for all analyzed wavelengths (Asufit). As a result of the analysis, the characteristic time constants were obtained as well as the wavelength-dependent amplitudes associated with them (also called decay associated difference spectra or pre-exponential factor spectra).

It should be noted that the cells measured by transient absorption and electrochemical impedance methods were assembled in two different laboratories with varying conditions. Therefore, it is difficult to directly compare the absolute efficiencies of the cells used for transient absorption with those measured by impedance spectroscopy.

Acknowledgements

This work was supported by NCN (National Science Centre, Poland) under project 2015/18/E/ST4/00196. J.S. is a holder of a scholarship funded within Human Capital Operational Programme, European Social Fund. Katarzyna Pydzińska is kindly acknowledged for help with the preparation and characterization of one series of ADEKA-1 cells. We would also like to thank Dr. Juan-Pablo Correa-Baena for help with preparation of some ALD layers and Prof. Shaik Mohammed Zakeeruddin for help with interpretation of the results.

Keywords: dyes/pigments · cobalt-based electrolytes · dye-sensitized solar cells · time-resolved laser spectroscopy

[1] A. Hagfeldt, G. Boschloo, L. Sun, L. Kloo, H. Pettersson, *Chem. Rev.* **2010**, *110*, 6595 – 6663.
[2] M. Grätzel, *Nature* **2001**, *414*, 338 – 344.
[3] M. Grätzel, J. R. Durrant, in *Nanostructured and Photoelectrochemical Systems for Solar Photon Conversion* (Eds.: M. D. Archer, A. J. Nozik), Imperial College Press, **2008**, pp. 503 – 536.
[4] K. Kalyanasundaram, *Dye-Sensitized Solar Cells*, EPFL Press, **2010**.
[5] www.nrel.gov/ncpv, National Renewable Energy Laboratory (NREL).
[6] J. Sobuś, M. Ziółek, *Phys. Chem. Chem. Phys.* **2014**, *16*, 14116 – 141126.
[7] B. O'Regan, M. Grätzel, *Nature* **1991**, *353*, 737 – 740.
[8] M. K. Nazeeruddin, F. De Angelis, S. Fantacci, A. Selloni, G. Viscardi, P. Liska, S. Ito, B. Takeru, M. Grätzel, *J. Am. Chem. Soc.* **2005**, *127*, 16835 – 16847.
[9] Q. Yu, Y. Wang, Z. Yi, N. Zu, J. Zhang, M. Zhang, P. Wang, *ACS Nano* **2010**, *4*, 6032 – 6038.
[10] S. M. Feldt, G. Wang, G. Boschloo, A. Hagfeldt, *J. Phys. Chem. C* **2011**, *115*, 21500 – 21507.
[11] D. Zhou, Q. Yu, N. Cai, Y. Bai, Y. Wang, P. Wang, *Energy Environ. Sci.* **2011**, *4*, 2030 – 2034.
[12] M. Pazoki, P. W. Lohse, N. Taghavinia, A. Hagfeldt, G. Boschloo, *Phys. Chem. Chem. Phys.* **2014**, *16*, 8503 – 8508.
[13] L. Giribabu, R. Bolligarla, M. Panigrahi, *Chem. Rec.* **2015**, *15*, 760 – 788.
[14] K. Lim, M. J. Ju, J. Na, H. Choi, M. Y. Song, B. Kim, K. Song, J.-S. Yu, E. Kim, J. Ko, *Chem. Eur. J.* **2013**, *19*, 9442 – 9446.
[15] K. D. Seo, I. T. Choi, H. K. Kim, *Chem. Eur. J.* **2015**, *21*, 14804 – 14811.
[16] A. Yella, H.-W. Lee, H. N. Tsao, C. Yi, A. K. Chandiran, M. K. Nazeeruddin, E. W.-G. Diau, C.-Y. Yeh, S. M. Zakeeruddin, M. Grätzel, *Science* **2011**, *334*, 629 – 634.
[17] S. Mathew, A. Yella, P. Gao, R. Humphry-Baker, B. F. E. Curchod, N. Ashari-Astani, I. Tavernelli, U. Rothlisberger, M. K. Nazeeruddin, M. Grätzel, *Nat. Chem.* **2014**, *6*, 242 – 247.
[18] F. Bella, N. Vlachopoulos, K. Nonomura, S. M. Zakeeruddin, M. Grätzel, C. Gerbaldia, A. Hagfeldt, *Chem. Commun.* **2015**, *51*, 16308 – 16311.
[19] F. Bella, S. Galliano, C. Gerbaldi, G. Viscardi, *Energies* **2016**, *9*, 384.
[20] K. Kakiage, T. Tokutome, S. Iwamoto, T. Kyomen, M. Hanaya, *Chem. Commun.* **2013**, *49*, 179 – 180.
[21] K. Kakiage, Y. Aoyama, T. Yano, T. Otsuka, T. Kyomen, M. Unno, M. Hanaya, *Chem. Commun.* **2014**, *50*, 6379 – 6381.
[22] S. K. Matta, K. Kakiage, S. Makuta, A. Veamatahau, Y. Aoyama, T. Yano, M. Hanaya, Y. Tachibana, *J. Phys. Chem. C* **2014**, *118*, 28425 – 28434.
[23] K. Kakiage, Y. Aoyama, T. Yano, K. Oya, T. Kyomen, M. Hanaya, *Chem. Commun.* **2015**, *51*, 6315 – 6317.
[24] K. Kakiage, Y. Aoyama, T. Yano, K. Oya, J.-i. Fujisawa, M. Hanaya, *Chem. Commun.* **2015**, *51*, 15894 – 15897.
[25] N. Koumura, Z.-S. Wang, S. Mori, M. Miyashita, E. Suzuki, K. Hara, *J. Am. Chem. Soc.* **2006**, *128*, 14256 – 14257.
[26] T. N. Murakami, N. Koumura, T. Uchiyama, Y. Uemura, K. Obuchi, N. Masaki, M. Kimurac, S. Mori, *J. Mater. Chem. A* **2013**, *1*, 792 – 798.
[27] M. K. Kashif, J. Axelson, N. W. Duffy, C. M. Forsyth, C. J. Chang, J. R. Long, L. Spiccia, U. Bach, *J. Am. Chem. Soc.* **2012**, *134*, 16646 – 16653.
[28] K. Hara, Z.-S. Wang, Y. Cui, A. Furube, N. Koumura, *Energy Environ. Sci.* **2009**, *2*, 1109 – 1114.
[29] M.-C. Brochier Salon, M. Naceur Belgacem, *Phosphorus Sulfur Silicon* **2011**, *186*, 240 – 254.
[30] K. J. McNeil, J. A. DiCaprio, D. A. Walsh, R. F. Pratt, *J. Am. Chem. Soc.* **1980**, *102*, 1859 – 1865.
[31] P. Van Der Voorta, E. F. Vansanta, *J. Liq. Chromatogr. Relat. Technol.* **1996**, *19*, 2723 – 2752.
[32] J. W. Goodwin, R. S. Harbron, P. A. Reynolds, *Colloid Polym. Sci.* **1990**, *268*, 766 – 777.
[33] T. Deschner, Y. Liang, R. Anwander, *J. Phys. Chem. C* **2010**, *114*, 22603 – 22609.
[34] J. Sobuś, J. Kubicki, G. Burdziński, M. Ziółek, *ChemSusChem* **2015**, *8*, 3118 – 3128.
[35] M. Lorenc, M. Ziółek, R. Naskręcki, J. Karolczak, J. Kubicki, A. Maciejewski, *Appl. Phys. B* **2002**, *74*, 19.
[36] X.-H. Zhang, J. Ogawa, K. Sunahara, Y. Cui, Y. Uemura, T. Miyasaka, A. Furube, N. Koumura, K. Hara, S. Mori, *J. Phys. Chem. C* **2013**, *117*, 2024 – 2031.
[37] J. Wiberg, T. Marinado, D. P. Hagberg, L. Sun, A. Hagfeldt, B. Albinsson, *J. Phys. Chem. B* **2010**, *114*, 14358 – 14363.
[38] P. Piatkowski, C. Martin, M. R. di Nunzio, B. Cohen, S. Pandey, S. Hayse, A. Douhal, *J. Phys. Chem. C* **2014**, *118*, 29674 – 29687.
[39] W.-K. Huang, C.-W. Cheng, S.-M. Chang, Y.-P. Lee, E. W.-G. Diau, *Chem. Commun.* **2010**, *46*, 8992 – 8994.
[40] B.-G. Kim, K. Chung, J. Kim, *Chem. Eur. J.* **2013**, *19*, 5220 – 5230.
[41] T. Debnath, P. Maity, H. Lobo, B. Singh, G. S. Shankarling, H. N. Ghosh, *Chem. Eur. J.* **2014**, *20*, 3510 – 3519.

[42] H. Imahori, S. Kang, H. Hayashi, M. Haruta, H. Kurata, S. Isoda, S. E. Canton, Y. Infahsaeng, A. Kathiravan, T. Pascher, P. Chábera, A. P. Yartsev, V. Sundström, *J. Phys. Chem. A* **2011**, *115*, 3679–3690.

[43] S. Ye, A. Kathiravan, H. Hayashi, Y. Tong, Y. Infahsaeng, P. Chabera, T. Pascher, A. P. Yartsev, S. Isoda, H. Imahori, V. Sundström, *J. Phys. Chem. C* **2013**, *117*, 6066–6080.

[44] S. Ardo, Y. Sun, A. Staniszewski, F. N. Castellano, G. J. Meyer, *J. Am. Chem. Soc.* **2010**, *132*, 6696–6709.

[45] U. B. Cappel, S. M. Feldt, J. Schöneboom, A. Hagfeldt, G. Boschloo, *J. Am. Chem. Soc.* **2010**, *132*, 9096–9101.

[46] G. Burdziński, J. Karolczak, M. Ziółek, *Phys. Chem. Chem. Phys.* **2013**, *15*, 3889–3896.

[47] T. Yoshihara, R. Katoh, A. Furube, Y. Tamaki, M. Murai, K. Hara, S. Murata, H. Arakawa, M. Tachiya, *J. Phys. Chem. B* **2004**, *108*, 3817–3823.

[48] Y. Tamaki, K. Hara, R. Katoh, M. Tachiya, A. Furube, *J. Phys. Chem. C* **2009**, *113*, 11741–11746.

[49] J. Sobuś, J. Karolczak, D. Komar, J. A. Anta, M. Ziółek, *Dyes Pigm.* **2015**, *113*, 692–701.

[50] C. Martín, M. Ziółek, A. Douhal, *J. Photochem. Photobiol. C* **2016**, *26*, 1–30.

[51] I. Iatsunskyi, E. Coy, R. Viter, G. Nowaczyk, M. Jancelewicz, I. Baleviciute, K. Załęski, S. Jurga, *J. Phys. Chem. C* **2015**, *119*, 20591–20599.

[52] F. Fabregat-Santiago, G. Garcia-Belmonte, I. Mora-Seró, J. Bisquert, *Phys. Chem. Chem. Phys.* **2011**, *13*, 9083–9118.

[53] J. Idígoras, G. Burdziński, J. Karolczak, J. Kubicki, G. Oskam, J. A. Anta, M. Ziółek, *J. Phys. Chem. C* **2015**, *119*, 3931–3944.

[54] E. Katilius, J. Hindorff, N. Woodbury, p. ASUFIT program available at www.public.asu.edu/~laserweb/asufit/asufit.html.

Received: June 27, 2016

FULL PAPER

Pressing charges: Time-resolved techniques were employed to study the impact of key preparation factors on the partial charge separation efficiencies in ADEKA-1 solar cells. Unwanted recombination of electrons from titania to this alkoxysilyl-anchor dye results in the lowering of residual signal at long delays.

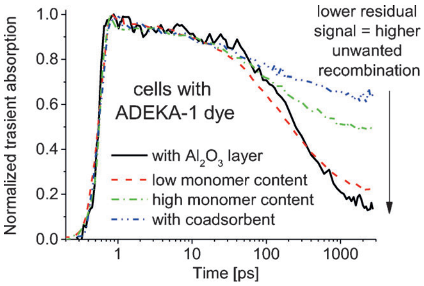

Physical Chemistry

*J. Sobuś, B. Gierczyk, G. Burdziński, M. Jancelewicz, E. Polanski, A. Hagfeldt, M. Ziółek**

■■ – ■■

Factors Affecting the Performance of Champion Silyl-Anchor Carbazole Dye Revealed in the Femtosecond to Second Studies of Complete ADEKA-1 Sensitized Solar Cells